AIP Journal of Applied Physics

Spin-phonon interactions of multiferroic Bi4Ti3O12-BiFeO3 ceramics: Low-temperature Raman scattering and infrared reflectance spectra investigations

P. P. Jiang, X. L. Zhang, P. Chang, Z. G. Hu, W. Bai, Y. W. Li, and J. H. Chu

Citation: Journal of Applied Physics **115**, 144101 (2014); doi: 10.1063/1.4870054
View online: http://dx.doi.org/10.1063/1.4870054
View Table of Contents: http://scitation.aip.org/content/aip/journal/jap/115/14?ver=pdfcov
Published by the AIP Publishing

Spin-phonon interactions of multiferroic $Bi_4Ti_3O_{12}$-$BiFeO_3$ ceramics: Low-temperature Raman scattering and infrared reflectance spectra investigations

P. P. Jiang (姜鹏鹏), X. L. Zhang (张小龙), P. Chang (常平), Z. G. Hu (胡志高),[a)]
W. Bai (白伟), Y. W. Li (李亚巍), and J. H. Chu (褚君浩)
Department of Electronic Engineering, Key Laboratory of Polar Materials and Devices, Ministry of Education, East China Normal University, Shanghai 200241, China

(Received 17 February 2014; accepted 19 March 2014; published online 8 April 2014)

Optical phonons of multiferroic $Bi_4Ti_3O_{12}$-$BiFeO_3$ ceramic have been investigated by low temperature Raman scattering and infrared reflectance spectra. Anomalies at about 85 K can be observed from the temperature dependence of the Raman and infrared modes, which arise from spin-phonon interaction during antiferromagnetic to paramagnetic phase transition. It was found that the change of exchange interaction in magnetic phase transition can be induced by Fe-O-Fe octahedral tilting driven from the *A*-site atoms. Moreover, ferroelectricity-related displacement of Bismuth atoms suggests the coupling of magnetic and ferroelectric orders. © *2014 AIP Publishing LLC*. [http://dx.doi.org/10.1063/1.4870054]

I. INTRODUCTION

$Bi_4Ti_3O_{12}$-$BiFeO_3$ ($Bi_5Ti_3FeO_{15}$, BTF) ceramics have great potential applications in non-volatile memories and high-temperature piezoelectric materials because of remarkable multiferroic, lead-free and fatigue-free properties, and high Curie temperature (T_c).[1,2] BTF belongs to Aurivillius family of the bismuth layer structured compounds with general formula $(Bi_2O_2)^{2+}(A_{n-1}B_nO_{3n-1})^{2-}$, where: $n=4$, A = Bi cations and B = Ti/Fe cations.[3,4] Compared with the highly competitive multiferroic $BiFeO_3$, the layer structured BTF can substantially reduce leakage current and reach high resistivity at room temperature (RT) because Fe-centered octahedron is inserted into two adjacent Bi-O layers. BTF ceramic presents a coexistence of antiferromagnetic (AFM) and ferroelectric (FE) order parameters: an AFM Néel temperature (T_N) of about 80 K (Ref. 5) and a FE T_c of about 1023 K.[6] The coupling between AFM and FE properties makes it possible for manipulating electrical property through magnetic fields and vice versa. The systematical investigations on two typical phase transitions are necessary to further clarify magnetoelectric coupling phenomena of multiferroic oxides.

There have been several reports on the magnetic order of $Bi_4Ti_3O_{12}$-$BiFeO_3$ system. BTF ceramic presents AFM order in the low temperature, which originates from Fe-O-Fe superexchange interaction.[5,7] However, the random distribution of Fe/Ti-centered octahedra in the perovskite-like slabs forms the local AFM order rather than long-range AFM order. On the other hand, BTF presents paramagnetic (PM) order beyond 80 K according to nearly linear M-H relationship.[8] Nevertheless, the physical mechanism of AFM to PM phase transition still remains ambiguous, which is a challenging problem for further exploitation of multiferroics-based device applications. Microscopic nature of the phase transition is required for the optimization of multiferroic properties, which can be better understood through the studies of optical excitations such as temperature dependent infrared active modes due to spin-lattice interaction.[9] However, few reports about thermal-optical responses and lattice vibrations of BTF ceramic during AFM to PM magnetic phase transition have been presented to date. As we know, both of Raman scattering and infrared reflectance spectra are nondestructive and attractive probe techniques, which are complementary and can provide some invaluable information on lattice vibrations and structural variations.[10] The information can be used to resolve the question of whether the phonon changes during the magnetic transition mainly arise from spin-reorientation, through spin-phonon coupling, and/or from the structural variations.

In this work, Raman scattering combined with Fourier transform infrared (FTIR) reflectance spectral experiments have been carried out in the temperature range of 3.6/5.5–300 K. The remarkable variations of optical phonon modes during the magnetic transition have been discussed to elucidate the spin-phonon coupling and the effect of A-site atom vibrations during the AFM-PM phase transition for BTF ceramic.

II. EXPERIMENTAL DETAILS

$Bi_4Ti_3O_{12}$-$BiFeO_3$ ceramic was synthesized using a conventional solid state reaction method. The TiO_2, Fe_2O_3, and Bi_2O_3 powders as precursor materials with 3 wt. % excess Bi_2O_3 to compensate the Bi volatilization were ball milled together in ethanol for 24 h, presintered at 800 °C for 6 h, and then ball milled again for 24 h. At last, the pretreated powders were pressed into small pellets and sintered at 1050 °C for 240 min. The details of fabricating process can be found in Ref. 7. Before spectral measurements, the ceramic was rigorously double-side polished and cleaned in pure ethanol with an ultrasonic bath and rinsed several times by deionized water. The phase and crystal structures of BTF ceramic were

[a)]Author to whom correspondence should be addressed. Tel.: +86-21-54345150. Fax: +86-21-54345119. Electronic mail: zghu@ee.ecnu.edu.cn

determined by X-ray diffraction (XRD) using Cu $K\alpha$ radiation (D/MAX-2550 V, Rigaku Co.), which indicates that the BTF ceramic is polycrystalline without impurity phases at RT.

Temperature-dependent infrared reflectance spectra were recorded by a Bruker VERTEX 80 V FTIR spectrometer equipped with a specular reflectance setup. The incident angle was set to about 6°. The far-infrared (FIR) spectra were measured in the frequency range of 70–450 cm^{-1} by a globar lamp (an U-shaped SiC piece), a 6 μm Mylar beamsplitter, and a pyroelectric DLaTGS detector. Meanwhile, a globar source (SiC), a KBr beamsplitter, and DLaTGS detector were used to measure the mid-infrared spectra from 450 to 1000 cm^{-1}. BTF ceramic was mounted into an Oxford AC-V12w continuous flow cryostat with the ceramic sample in He vapor. The temperature can be varied from 5.5 to 300 K. The cryostat was equipped with polypropylene and ZnSe windows for the FIR and mid-infrared (MIR) regions, respectively. The spectral resolution is set to 2 cm^{-1}. On the other hand, temperature-dependent Raman scattering measurements were carried out by a Jobin-Yvon LabRAM HR800 UV micro-Raman spectrometer. The He-Ne laser with the wavelength of 632.8 nm is taken as the exciting source. The laser beam was focused through a 50× microscope with a working distance of 18 mm. An air-cooled charge coupled device (CCD) (−70 °C) with a 1024 × 256 pixels front illuminated chip was used to collect the scattered signal dispersed on 1800 grooves/mm grating.[10] The $Bi_4Ti_3O_{12}$-$BiFeO_3$ ceramic was mounted into a continuous flow liquid helium cryostat (Oxford cryostat MicrostathiresII system). The temperature can be controlled in the range of 3.6-300 K with a precision of about 0.5 K.

III. RESULTS AND DISCUSSION

Fig. 1 shows temperature-dependent Raman spectra of the BTF ceramic from 3.6 to 300 K. Note that Raman spectra are plotted in logarithmic scale in order to clarify the temperature dependence of Raman modes located at low frequencies. The modes located at about 265 and 864 cm^{-1} with A_{1g} character show no obvious shift with the temperature, which indicates that $(Ti/Fe)O_6$ octahedra cannot present any torsionally bending or stretching behaviors during the magnetic phase transition.[8] Moreover, the mode located at 459 cm^{-1} is related to the variation of the bond distances between the Bi atoms within Bi_2O_2 layer and the apical O atoms of the perovskite-like block. The modes at about 543 and 573 cm^{-1} can be ascribed to the opposite vibration of the apical O atoms at the top of $(Ti/Fe)O_6$ octahedra.[11] All of them show no apparent shift except for the degeneration trend due to the thermal expansion. Note that the modes at about 62 and 124 cm^{-1} (labeled by "diamond") remain nearly invariant until about 85 K and then show a dramatically red shift beyond 85 K. These modes are related to the vibrations of Bi atoms. As we know, the magnetic phase transition is too subtle to be accompanied by these observable phonon anomalies. The similar scenario will be seen in the following discussion on the results of infrared reflectance. The possible origins of the anomalies at T_N can be summarized as follows: (1) magnetostriction; (2) spin and phonon degrees of freedom coupling; and (3) magnetic and ferroelectric order parameter coupling.[12] The changes of the lattice constants, produced by magnetostriction, are much smaller than the effects of thermal expansion and can be ignored. In the present work, the spin-phonon and magnetic-ferroelectric order parameter couplings can be verified through the thermal evolution of Raman- and infrared-active modes.

Next, temperature-dependent infrared reflectance spectra from 5.5 to 300 K are plotted in Fig. 2. The insets in Fig. 2(a) show the detailed degenerated trend of infrared bands from the experimental spectra. As we can see, these peaks located at 146, 396, 470, and 694 cm^{-1} present a degraded trend, indicating the disorder of atomic vibrations with increasing the temperature. Moreover, these peaks originate from spin-phonon interaction in AFM order and the disappearance of the interaction in PM phase results in the degeneration.[13] By combining with the results from Raman spectra, the mode "I" can be assigned to translational motions of the Bi^{3+}, the mode "II" is related to Ti-O-Ti/Fe

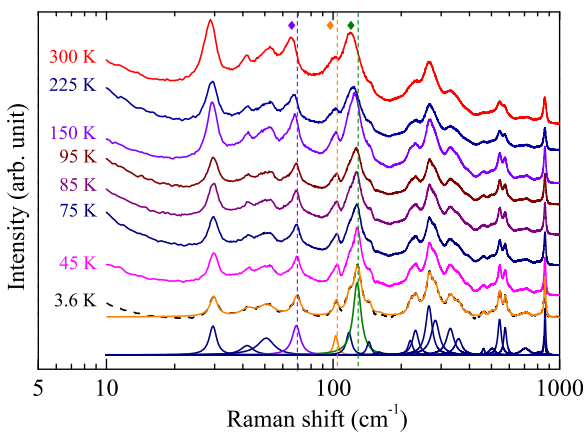

FIG. 1. Raman spectra in the range of 10–1000 cm^{-1} recorded from 3.6 to 300 K for $Bi_4Ti_3O_{12}$-$BiFeO_3$ ceramic. It can be noted that the modes marked by "diamond" at 128, 103, and 69 cm^{-1} present more obvious red shift trend beyond 85 K. The well-fitted Raman spectrum at 3.6 K is given as an example.

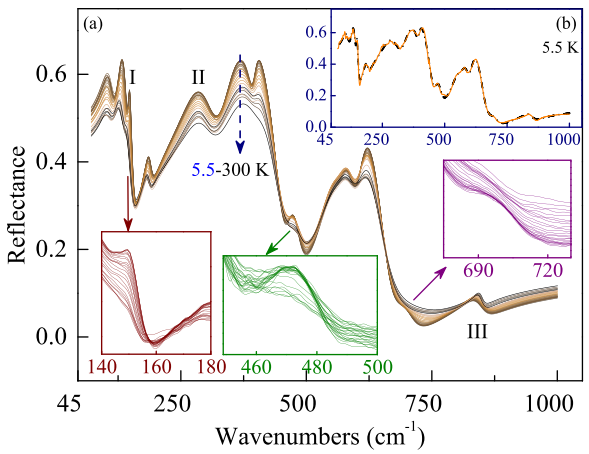

FIG. 2. (a) Low-temperature infrared reflectance spectra of $Bi_4Ti_3O_{12}$-$BiFeO_3$ ceramic in the frequency range of 70–1000 cm^{-1}. Note that the insets represent the experimental data. The labels "I," "II," and "III" show three well-defined modes: Bi atomic vibrations in perovskite like blocks, Ti-O-Ti/Fe bending, and Ti-O stretching, respectively. (b) The well-fitted infrared reflectance spectrum at 5.5 K is given as an example.

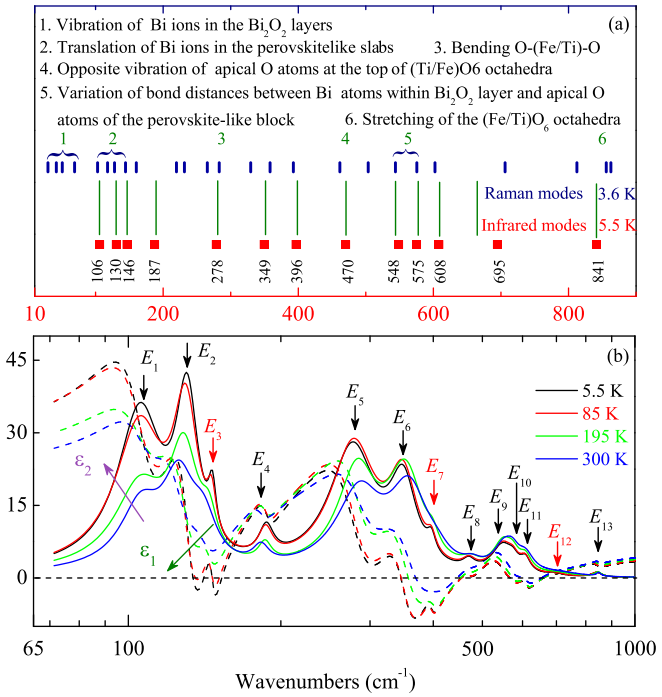

FIG. 3. (a) Comparison of Raman-active and infrared-active modes for $Bi_4Ti_3O_{12}$-$BiFeO_3$ ceramic with the proposed assignment. Phonon frequencies from Raman scattering are in the range of 10–1000 cm^{-1} and phonon frequencies from infrared reflectance spectra are in the range of 70–1000 cm^{-1}, respectively. Note that there are 25 and 13 modes derived from the fitting process for Raman scattering and infrared reflectance, respectively. (b) Dielectric dispersion functions for $Bi_4Ti_3O_{12}$-$BiFeO_3$ ceramic at 5.5, 85, 195, and 300 K, respectively. Note that horizontal direction is linear coordinate in Fig. 3(a) and logarithmic coordinate in Fig. 3(b), respectively.

bending and the mode "III" is associated with the Ti/Fe-O stretching.[14–16] Note that the well-defined modes "II" and "III" for BTF ceramic are corresponding to Raman modes at 265 and 864 cm^{-1}, respectively. The frequencies of the modes "II" and "III" have a typical linear temperature dependence and the reflection intensity of these modes presents a decreasing trend with increasing the temperature, which agrees well with the results of Raman scattering.

To better study the AFM to PM phase transition, fitting procedures were carried out. Raman and infrared active-modes in the low temperature with the proposed assignments are plotted in Fig. 3(a) for comparison. We can discern 25 and 13 modes for Raman scattering and infrared reflection, respectively. In the fitting process, Raman spectra were corrected for the Bose-Einstein temperature factor to eliminate the contribution of the Bose Einstein population factor from the measured Raman intensity. The reduced Raman intensity is written as $R(\nu) = I(\nu)/[n(\nu)+1]$, where $I(\nu)$ corresponds to the measured Raman intensity and $n(\nu) = (e^{h\nu/kT}\text{-}1)^{-1}$ is the Bose-Einstein factor.[17] Note that the oscillator at about 117 cm^{-1} can be ignored beyond the point T_N of 85 K during the fitting process. Correspondingly, the analysis of temperature-dependent infrared reflectance spectra was carried out in order to investigate the change of infrared-active phonon modes with the magnetic transition. Infrared spectra are fitted to classical Lorentz dispersion model written as follow:

$$\varepsilon(\omega) = \varepsilon_\infty + \sum_{j=1}^{m} \frac{A_j E_j^2}{E_j^2 - \omega^2 - iBr_j\omega}. \quad (1)$$

Here, ε_∞ is the high frequency dielectric constant. ω is the frequency of incident light. A_j, E_j, and Br_j denote the phonon strength, the phonon frequency, and the broadening, respectively. In the fitting process, thirteen oscillators ($m = 13$) were used to reproduce infrared reflectance bands well. The best-fitting parameters from the Lorentz model at three typical temperatures are given in Table I. The well-fitted Raman and infrared spectra can be seen in Figs. 1 and 2, respectively. Moreover, the dielectric functions can be abstracted through the Fresnel's formula: $R = |(\sqrt{\varepsilon(\omega)}-1)/(\sqrt{\varepsilon(\omega)}+1)|^2$. The real part ε_1 and imaginary part ε_2 of dielectric functions at 5.5, 85, 195, and 300 K are plotted in Fig. 3(b). Dielectric functions have a relatively weak temperature dependence below 85 K. The phonon modes are well defined by E_{1-13} in the order of increasing the frequency. Note that E_3, E_7, and E_{12} cannot be well resolved beyond $T_N = 85$ K. The modes E_{1-4} at low frequencies show a typical red shift with the temperature. The red shift becomes more obvious beyond about 85 K because of the statistical increase of the number of acoustic phonons.

Fig. 4 shows the temperature dependence of phonon frequencies and full width at half maximum (FWHM) of some interesting Raman modes. First, the normally thermal evolution of the mode at 103 cm^{-1} has been plotted, for example, which can be ascribed to the thermal expansion of the lattice and anharmonic phonon-phonon interactions.[18] On the other hand, the mode located at 128 cm^{-1} under 3.6 K gradually shift to 120 cm^{-1} with increasing the temperature. One can clearly see the more obvious red shift beyond 85 K. The red shift cannot be just explained by the temperature effect. The anomalies observed in Fig. 4 are visible in the experimentally measured Raman spectra labeled by "diamond" in Fig. 1. The abnormal phonon shifts can be explained in terms of the change in the effective restoring force, which is coming from modulation of the exchange energy during the spin-reorientation.[19] The exchange energy mainly originates from the superexchange of Fe-O-Fe interaction. Note that both of the modes at 103 and 128 cm^{-1} originate from the vibration of A-site atoms (Bi) in the perovskite-like slabs. It indicates that the motions of the A-site atoms have great influence on superexchange between nearest-neighbor Fe ions separated by oxygen. The variation between Bi and O atoms in Fe-O-Fe chains results in the tilting of Fe-O-Fe octahedra, which breaks down the ordered superexchange interaction and causes the AFM to PM magnetic phase transition around 85 K. The octahedral tilt shows that there is discernable interaction between the magnetic order parameter and octahedral tilting.[20] Therefore, the substitution of A-site atoms (i.e., niobium) can effectively tilt the iron-oxygen octahedra and release the latent magnetization locked in the AFM order, which could enhance its magnetic properties.[21,22] On the other hand, it is known that the displacement of Bi ions in the perovskite-like blocks is closely associated with the ferroelectricity.[23] The phenomena indicate the possible coupling between magnetic and ferroelectric order parameters.

TABLE I. The Lorentz oscillator model parameters for $Bi_4Ti_3O_{12}$-$BiFeO_3$ ceramic extracted from the best-fitting infrared reflectance spectra at 5.5, 85, and 300 K, respectively. The 90% reliability is given in parentheses.

			Phonon modes												
Temperature (K)	Parameters	ε_∞	E_1	E_2	E_3	E_4	E_5	E_6	E_7	E_8	E_9	E_{10}	E_{11}	E_{12}	E_{13}
5.5	A	5.19	31.8	34	10.5	6.3	25.4	18	3.73	1.86	5.78	1.81	2.71	0.5	0.95
		(0.02)	(0.98)	(1.13)	(0.68)	(0.41)	(0.29)	(0.3)	(0.18)	(0.39)	(0.31)	(0.39)	(0.1)	(0.02)	(0.04)
	E (cm^{-1})		106	131	147	187	279	350	397	470	549	575	608	695	842
			(0.6)	(0.3)	(0.7)	(0.5)	(0.6)	(0.5)	(0.5)	(0.4)	(1.6)	(1.4)	(0.5)	(1.3)	(1.2)
	Br (cm^{-1})		25.6	16.3	6.3	15.5	70.7	53.4	19.1	31.5	65.2	34.5	33.7	54.4	47.5
			(2.09)	(1.14)	(0.77)	(1.66)	(1.98)	(1.78)	(1.76)	(1.69)	(2.46)	(6.77)	(1.28)	(5.02)	(3.7)
85	A	5.4	28.5	31.6	8.8	5.77	25.8	19	3.49	1.83	6.01	1.78	2.73	0.51	0.95
		(0.02)	(0.9)	(1.15)	(0.64)	(0.38)	(0.29)	(0.3)	(0.18)	(0.05)	(0.29)	(0.38)	(0.09)	(0.02)	(0.04)
	E (cm^{-1})		106	130	146	187	280	350	397	471	549	575	608	696	842
			(0.7)	(0.3)	(0.3)	(0.5)	(0.6)	(0.4)	(0.5)	(0.4)	(1.6)	(1.2)	(0.5)	(1.4)	(1.1)
	Br (cm^{-1})		27.5	18.2	7.26	15.1	69.2	56.3	19.9	34	65.9	32.7	36.1	64	46.6
			(2.41)	(1.36)	(0.98)	(1.66)	(1.86)	(1.72)	(1.94)	(1.82)	(2.46)	(6.05)	(1.28)	(5.57)	(3.33)
300	A	6	11.9	17.7	8.4	3.59	15.6	17.2	2.01	1.4	5.12	2.64	3.29	0.72	0.69
		(0.02)	(1.89)	(2.69)	(2.84)	(0.3)	(0.47)	(0.58)	(0.8)	(0.12)	(1.46)	(1.68)	(0.27)	(0.04)	(0.06)
	E (cm^{-1})		106	126	141	183	287	360	407	477	552	574	609	713	848
			(1.6)	(1)	(1.4)	(0.7)	(1.1)	(1.1)	(3.6)	(1.2)	(5.3)	(3.2)	(1.3)	(4.1)	(0.9)
	Br (cm^{-1})		23.1	23.1	20.3	16.4	71.2	79.1	53.2	48.4	63.8	43	55	177	20.1
			(4.24)	(5.94)	(3.69)	(2.38)	(3.09)	(5.96)	(13.4)	(5.91)	(6.12)	(14.6)	(2.9)	(16.7)	(3.01)

The order and disorder of magnetic phase have a different interaction with ferroelectricity, which results in the different temperature-dependence of Bi atom vibration. The sharp A_{1g} [Bi] mode at 62 cm^{-1} is regarded as a rigid mode and the mode at 30 cm^{-1} is supposed to be a soft mode. Both of them are related to the displacement of Bi ions within the Bi_2O_2 layers.[24] The FWHM of the mode at 62 cm^{-1} increases linearly with the temperature and then remains unchanged beyond 85 K, which suggests that the vibration of Bi ions in the Bi_2O_2 layers is insensitive to the temperature in the PM order.[25] The Bi_2O_2 layers play an important role in reducing leakage current and improve the anti-fatigue property. However, the increment of FWHM for the phonon modes located at 128 and 103 cm^{-1} indicates that the Bi atoms in the perovskite-like slabs can be easily thermally disturbed.

The variations of infrared-active mode frequencies and their broadenings for BTF ceramic from 5.5 to 300 K are depicted in Fig. 5. As we can see in Fig. 2, the modes at 146, 396, 470, and 694 cm^{-1} gradually disappear with the

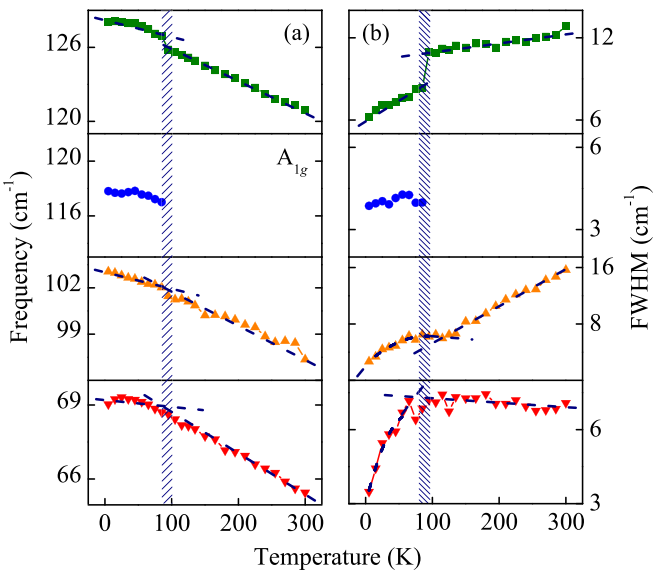

FIG. 4. Temperature dependence of Raman-active modes at 69, 103, 118, and 128 cm^{-1} from $Bi_4Ti_3O_{12}$-$BiFeO_3$ ceramic: (a) Phonon frequency and (b) the corresponding FWHM. Note that the values of FWHM increase with the temperature except for the Raman mode at about 69 cm^{-1}, which remains stable beyond 85 K.

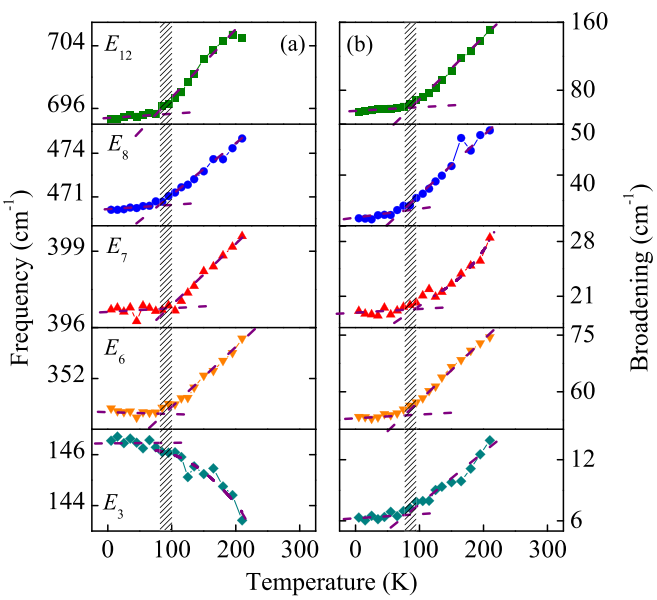

FIG. 5. Temperature evolution of infrared-active modes at 147, 350, 397, 470, and 695 cm^{-1} from $Bi_4Ti_3O_{12}$-$BiFeO_3$ ceramic: (a) Phonon frequency and (b) the corresponding broadening value. Note that the distinct variation trends appear across the Néel temperature of about 85 K.

temperature, which are difficult to be fitted out accurately beyond 210 K. Hence, the thermal evolutions of these modes beyond 210 K are not presented. It is found that all broadening values remain nearly unchanged lower than 85 K and then increase obviously with the temperature. The phenomena can be ascribed to the competition between the thermal disturbance and the interaction of Fe-O-Fe magnetic moments. The AFM order is stable and sustained by the spin-phonon interaction at low temperature, while the thermal disturbance breaks down the balance and gives rise to spin re-orientation of PM magnetic moments with increasing the temperature. Hence, the thermal evolution of phonon broadenings can be reasonably explained by the magnetic-related order to disorder phase transition. The temperature dependence of infrared modes at about 146, 349, 396, 470, and 694 cm^{-1} lower than 85 K is different with the trend beyond 85 K, which confirms the spin-phonon interactions. The mode at 146 cm^{-1} is related to Bi-O vibrations, which plays an important role in the magnetic phase transition. For the other modes of infrared reflectance spectra, more experimental and theoretical works are necessary to realize the assignments in the future.

IV. CONCLUSIONS

To summarize, thermal evolution of $Bi_4Ti_3O_{12}$-$BiFeO_3$ ceramic has been investigated by Raman scattering and infrared reflectance in the temperature range of 3.6/5.5 K to 300 K. The antimagnetic to paramagnetic phase transition around 85 K is verified through the change of phonon frequencies and FWHM/broadenings due to spin-phonon interactions. The magnetic transition is caused by the change of exchange interaction, which can be well explained by A-site atoms (Bi) motivated tilting of Fe-O-Fe octahedral chains. Moreover, the magnetic-ferroelectric couplings can be well revealed during the magnetic phase transition.

ACKNOWLEDGMENTS

One of the authors (P. P. J.) would like to thank Dr. Xiao Chen and Dr. Kai Jiang for constructive discussions. This work was financially supported by Major State Basic Research Development Program of China (Grant Nos. 2011CB922200 and 2013CB922300), Natural Science Foundation of China (Grant Nos. 11374097, 61376129, and 61106122), Projects of Science and Technology Commission of Shanghai Municipality (Grant Nos. 13JC1402100 and 13JC1404200), and the Program for Professor of Special Appointment (Eastern Scholar) at Shanghai Institutions of Higher Learning.

[1]C. A. P. de Araujo, J. D. Cuchiaro, L. D. McMillan, M. Scott, and J. F. Scott, Nature (London) **374**, 627 (1995).
[2]T. Goto, T. Kimura, G. Lawes, A. P. Ramirez, and Y. Tokara, Phys. Rev. Lett. **92**, 257201 (2004).
[3]A. Srinivas, D. W. Kim, K. S. Hong, and S. V. Suryanarayana, Appl. Phys. Lett. **83**, 2217 (2003).
[4]P. F. Zhang, N. Deepak, L. Keeney, M. E. Pemble, and R. W. Whatmore, Appl. Phys. Lett. **101**, 112903 (2012).
[5]A. Srinivas, S. V. Suryanarayana, G. S. Kumar, and M. M. Kumar, J. Phys.: Condens. Matter **11**, 3335 (1999).
[6]J. B. Li, Y. P. Huang, G. H. Rao, G. Y. Liu, J. Luo, J. R. Chen, and J. K. Liang, Appl. Phys. Lett. **96**, 222903 (2010).
[7]G. Chen, W. Bai, L. Sun, J. Wu, Q. Ren, W. Xu, J. Yang, X. J. Meng, X. D. Tang, C. G. Duan, and J. H. Chu, J. Appl. Phys. **113**, 034901 (2013).
[8]X. Y. Mao, W. Wang, and X. B. Chen, Solid State Commun. **147**, 186 (2008).
[9]T. D. Kang, E. C. Standard, P. D. Rogers, K. H. Ahn, A. A. Sirenko, A. Dubroka, C. Bernhard, S. Park, Y. J. Choi, and S. W. Cheong, Phys. Rev. B **86**, 144112 (2012).
[10]X. Chen, Z. G. Hu, Z. H. Duan, X. F. Chen, G. S. Wang, X. L. Dong, and J. H. Chu, J. Appl. Phys. **114**, 043507 (2013).
[11]Y. L. Du, M. S. Zhang, Q. Chen, Z. R. Yuan, Z. Yin, and Q. A. Zhang, Solid State Commun. **124**, 113 (2002).
[12]R. Haumont, J. Kreisel, P. Bouvier, and F. Hippert, Phys. Rev. B **73**, 132101 (2006).
[13]S. Kamba, D. Nuzhnyy, M. Savinov, J. Sebek, J. Petzelt, J. Prokleška, R. Haumont, and J. Kreisel, Phys. Rev. B **75**, 024403 (2007).
[14]R. P. S. M. Lobo, R. L. Moreira, D. Lebeugle, and D. Colson, Phys. Rev. B **76**, 172105 (2007).
[15]R. L. Moreira, R. P. S. M. Lobo, G. Subodh, M. T. Sebastian, F. M. Matinaga, and A. Dias, Chem. Mater. **19**, 6548 (2007).
[16]M. Mączka, L. Macalik, K. Hermanowicz, L. Kępiński, and P. Tomaszewski, J. Raman Spectrosc. **41**, 1059 (2010).
[17]E. Buixaderas, I. Gregora, J. Hlinka, J. Dec, and T. Łukasiewicz, Phase Trans. **86**, 217 (2013).
[18]J. J. Zhu, W. W. Li, G. S. Xu, K. Jiang, Z. G. Hu, and J. H. Chu, Acta Mater. **59**, 6684 (2011).
[19]A. B. Souchkov, J. R. Simpson, M. Quijada, H. Ishibashi, N. Hur, J. S. Ahn, S. W. Cheong, A. J. Millis, and H. D. Drew, Phys. Rev. Lett. **91**, 027203 (2003).
[20]T. Y. Tan, B. J. Kennedy, Q. Zhou, C. D. Ling, W. Miiller, C. J. Howard, M. A. Carpenter, and K. S. Knight, Phys. Rev. B **85**, 104107 (2012).
[21]F. Z. Huang, X. M. Lu, C. Chen, W. W. Lin, X. C. Chen, J. T. Zhang, Y. F. Liu, and J. S. Zhu, Solid State Commun. **150**, 1646 (2010).
[22]X. Y. Mao, H. Sun, W. Wang, X. B. Chen, and Y. L. Lu, Appl. Phys. Lett. **102**, 072904 (2013).
[23]C. H. Hervoches, A. Snedden, R. Riggs, S. H. Kilcoyne, P. Manuel, and P. Lightfoot, J. Solid State Chem. **164**, 280 (2002).
[24]W. Wang, S. P. Gu, X. Y. Mao, and X. B. Chen, J. Appl. Phys. **102**, 024102 (2007).
[25]K. Jiang, W. W. Li, X. G. Chen, Z. N. Zhan, Z. G. Hu, and J. H. Chu, J. Raman Spectrosc. **43**, 583 (2012).